Capturing Ultrasmall EMT Zeolite from Template-Free Systems

Eng-Poh Ng, *et al.*

Science **335**, 70 (2012);
DOI: 10.1126/science.1214798

16. G. Manukyan, J. M. Oh, D. van den Ende, R. G. H. Lammertink, F. Mugele, *Phys. Rev. Lett.* **106**, 014501 (2011).
17. S. Herminghaus, *Europhys. Lett.* **52**, 165 (2000).
18. Q. Xie *et al.*, *Adv. Mater. (Deerfield Beach Fla.)* **16**, 302 (2004).
19. A. Tuteja, W. J. Choi, G. H. McKinley, R. E. Cohen, M. F. Rubner, *MRS Bull.* **33**, 752 (2008).
20. A. Steele, I. Bayer, E. Loth, *Nano Lett.* **9**, 501 (2009).
21. R. T. R. Kumar, K. B. Mogensen, P. Boggild, *J. Phys. Chem. C* **114**, 2936 (2010).
22. L. Joly, T. Biben, *Soft Matter* **5**, 2549 (2009).
23. A. Tuteja *et al.*, *Science* **318**, 1618 (2007).
24. A. Ahuja *et al.*, *Langmuir* **24**, 9 (2008).
25. L. Cao, T. P. Price, M. Weiss, D. Gao, *Langmuir* **24**, 1640 (2008).
26. C. M. Megaridis, R. A. Dobbins, *Combust. Sci. Technol* **71**, 95 (1990).
27. M. Callies, D. Quere, *Soft Matter* **1**, 55 (2005).
28. D. Bartolo *et al.*, *Europhys. Lett.* **74**, 299 (2006).
29. A. Tuteja, W. Choi, J. M. Mabry, G. H. McKinley, R. E. Cohen, *Proc. Natl. Acad. Sci. U.S.A.* **105**, 18200 (2008).
30. D. Richard, C. Clanet, D. Quéré, *Nature* **417**, 811 (2002).
31. M. Nosonovsky, *Langmuir* **23**, 3157 (2007).

Acknowledgments: We are grateful to G. Glaser, K. Kirchhoff, G. Schäfer, S. Pinnells, J. Ally, and P. Papadopoulos for technical support and stimulating discussions. We acknowledge financial support from Deutsche Forschungsgemeinschaft grants SPP 1273 (D.V.), SPP 1420 (H.J.B.), and SPP 1486 (L.M.).

Supporting Online Material

www.sciencemag.org/cgi/content/full/science.1207115/DC1
Materials and Methods
SOM Text
Figs. S1 to S11
Tables S1 and S2
References
Movies S1 to S3

8 April 2011; accepted 8 November 2011
Published online 1 December 2011;
10.1126/science.1207115

Capturing Ultrasmall EMT Zeolite from Template-Free Systems

Eng-Poh Ng,[1,2] Daniel Chateigner,[3] Thomas Bein,[4] Valentin Valtchev,[1] Svetlana Mintova[1]*

Small differences between the lattice energies of different zeolites suggest that kinetic factors are of major importance in controlling zeolite nucleation. Thus, it is critical to control the nucleation kinetics in order to obtain a desired microporous material. Here, we demonstrate how careful investigation of the very early stages of zeolite crystallization in colloidal systems can provide access to important nanoscale zeolite phases while avoiding the use of expensive organic templates. We report the effective synthesis of ultrasmall (6- to 15-nanometer) crystals of the large-pore zeolite EMT from template-free colloidal precursors at low temperature (30°C) and very high yield.

Zeolites are metastable crystalline aluminosilicate molecular sieves with uniform pores of molecular dimensions that are widely applied in catalysis, separations, and adsorption (*1*–*4*). The EMT-type zeolite has one of the lowest framework densities for a microporous material (*5*) and is a hexagonal polytype of the cubic FAU-type zeolite that plays a very important role in catalysis, for example, in fluid catalytic cracking (FCC) of hydrocarbons (*6*). Similar to the FAU-type material, the EMT framework topology has a three-dimensional large (12-membered ring) pore system. The cubic FAU polymorph features only one type of supercage (with a volume of 1.15 nm^3), but a different stacking of faujasite sheets creates two cages in the EMT zeolite: a hypocage (0.61 nm^3) and a hypercage (1.24 nm^3) (*7*). The EMT material shows interesting catalytic properties different from FAU as an FCC catalyst, but the very high price of the product so far precludes practical uses (*8*, *9*).

In addition, several EMT-FAU intergrown phases (CSZ-1, ECR-30, ZSM-20, ZSM-3) have also been reported (*9*–*14*). The synthesis of pure EMT-type zeolite is possible by templating with the expensive 18-crown-6 ether and using tightly controlled synthesis parameters (*7*). Many studies have been carried out to reduce the consumption of the crown ether template, for instance, by recycling after the synthesis (*15*) or using the so-called "SINTEF" tumbling approach (*16*, *17*), steam-assisted crystallization (*18*), surfactants (*19*), or other organic and inorganic auxiliary additives (*20*–*22*). Although the cost of producing EMT has been reduced, all attempts toward a synthesis of EMT-type zeolite without an organic structure-directing agent (OSDA) have been unsuccessful thus far. Moreover, the 18-crown-6 ether template stimulates the crystallization of micrometer-sized EMT crystals, and no attempts for the preparation of nanosized crystals have been reported.

Certain nanosized molecular sieves have been obtained at moderate (60° to 130°C) and low temperatures (25° to 50°C) (*23*–*26*). Low-temperature synthesis techniques for discrete zeolite nanocrystals from organic-free precursor systems are highly desired, as they would reduce cost and hazardous wastes, save energy, and possibly alter the properties of the materials (*26*, *27*). Here, we describe a template-free Na_2O–Al_2O_3–SiO_2–H_2O precursor system as a foundation for the preparation of a nanosized EMT molecular sieve, where the ratios between different compounds, nucleation temperature and times, and type of heating have been adjusted to avoid phase transformations (e.g., to FAU and SOD) and to stabilize the EMT-type crystals at a small particle size. We report the synthesis of ultrasmall hexagonal EMT nanocrystals (diameter of 6 to 15 nm) at the low temperature of 30°C without using any organic template; that is, from Na-rich precursor suspensions. Strikingly, this synthesis strategy requires no organic

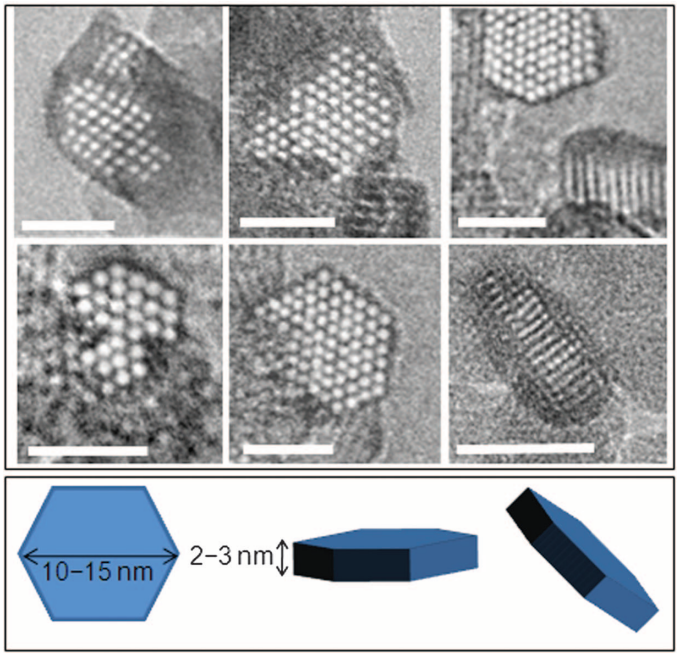

Fig. 1. Ultrasmall EMT crystals with hexagonal morphology synthesized from template-free precursor suspension at 30°C for 36 hours. The individual crystals are schematically presented with a size of 10 to 15 nm and a thickness of 2 to 3 nm. Scale bars, 10 nm.

[1]Laboratoire Catalyse and Spectrochimie, ENSICAEN, Université de Caen, CNRS, 6 Boulevard du Maréchal Juin, 14050 Caen, France. [2]School of Chemical Sciences, Universiti Sains Malaysia, 11800 USM, Pulau Pinang, Malaysia. [3]CRISMAT, ENSICAEN, Université de Caen, 6 boulevard du Maréchal Juin, 14050 Caen, France. [4]Department of Chemistry and Center for NanoScience, University of Munich (LMU), Butenandtstrasse 5-13 (E) Gerhard-Ertl-Building, 81377 Munich, Germany.

*To whom correspondence should be addressed. E-mail: svetlana.mintova@ensicaen.fr

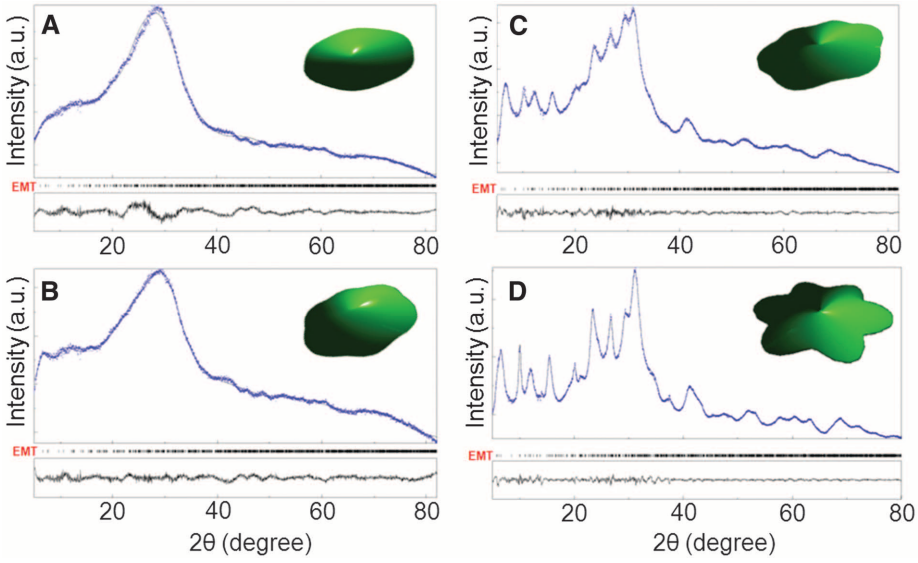

Fig. 2. XRD patterns representing the evolution of ultrasmall EMT crystals from template-free precursor suspensions at 30°C under conventional heating for (**A**) 8 hours, (**B**) 14 hours, (**C**) 24 hours, and (**D**) 36 hours. Vertical ticks correspond to line indexing of the EMT phase. The difference diagram between calculated and experimental points is shown at the bottom of each XRD pattern. (Insets) Crystallite sizes and shapes calculated based on the XRD data. The whole pattern was fitted using the combined analysis formalism (*30*) implemented in the MAUD program (*31*), based on the Rietveld analysis approach. Fourier analysis was applied to deconvolute the instrumental- and sample-broadening parts from the measured XRD lines. The instrumental contribution to the line broadening was calibrated with an LaB_6 standard powder from the National Institute of Standards and Technology. The Popa formalism was then used to describe anisotropic crystallite sizes and shapes (*32*), and an arbitrary texture correction model (*31*) was used to account for the moderate preferred orientations introduced in the EMT powder in a flat sample holder. a.u., arbitrary units.

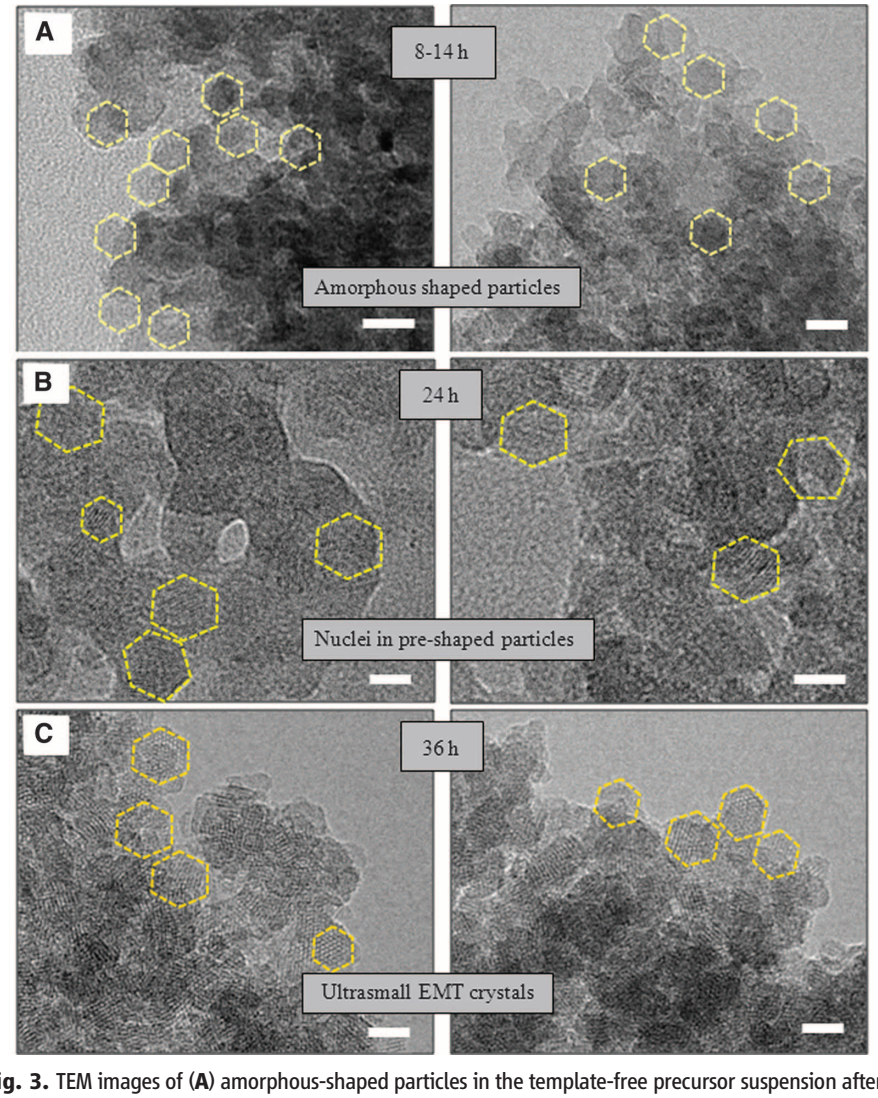

Fig. 3. TEM images of (**A**) amorphous-shaped particles in the template-free precursor suspension after 8 to 14 hours, (**B**) birth of ultrasmall EMT nuclei after 24 hours, and (**C**) fully crystalline ultrasmall EMT after 36 hours of conventional heating at 30°C. Scale bars, 10 nm.

template. Moreover, the absence of an organic template implies that no high-temperature calcination step is required for opening up the pore system for the intended applications.

Typically, a high concentration of OSDA is needed to prepare nanosized zeolites to achieve a high degree of supersaturation by which the crystal size can be controlled and the resulting nanoparticles can be stabilized. We synthesized the ultrasmall (6- to 15-nm) and nanosized (50- to 70-nm) EMT crystals at near ambient conditions within a very short time; that is, 36 hours under conventional heating and 4 min under microwave irradiation, respectively (see supporting online material, fig. S1). We used these "soft" conditions to avoid the formation of the more stable and denser phase hydroxysodalite (SOD) and the formation of a FAU-type phase observed in precursor suspensions with slight changes of the oxide ratios and water content (fig. S2).

The ultrasmall EMT crystals prepared at 30°C for 36 hours under conventional heating are shown in Fig. 1. Nearly 63% of the amorphous aluminosilicates were transformed into ultrasmall hexagonal EMT zeolite (Si/Al = 1.14). The particles were single crystals with a size of ~6 to 15 nm, and they contained channels in a highly ordered hexagonal arrangement. The x-ray diffraction (XRD) pattern of this sample (fully crystalline EMT-type zeolite) exhibited broadened Bragg peaks, which suggests the presence of very small crystallite sizes (Fig. 2D). The pattern was indexed using the hexagonal EMT structure in the $P6_3/mmc$ space group, with a reliability factor as low as weighted R_w = 1.5%, Bragg R_B = 1.12%, and experimental R_{exp} = 0.62%, which gave rise to a goodness-of-fit of 6. In addition, zeolites X and Y (FAU-type structures) were considered in the modeling; however, they did not fit the first three peaks characteristic of the EMT zeolite, nor the anisotropic line broadening (fig. S3).

The refined cell parameters, a = 1.7616(1) nm and c = 2.838(2) nm, correspond very well to the EMT-type structure (*5*). Moreover, the refined shape of the particles was a hexagonal crystal with mean sizes of 10 nm along the [100] direction, 15 nm along [110], and 2.0 nm along [001]. The refined shape of the crystallites matched the size and shape of the EMT crystals measured with high-resolution transmission electron microscopy (HRTEM) (Figs. 1 and 2D). Moreover, the fitting of this XRD pattern (sample synthesized at 30°C for 36 hours) with isotropic and platelike EMT crystals did not provide better fitting results (fig. S3 and table S1).

We investigated the entire process of nucleation and growth of the ultrasmall EMT crystals in the system subjected to conventional heating for a total period of 36 hours. HRTEM images of the solid particles extracted at different crystallization times revealed the presence of amorphous gel after 8 to 14 hours and fully crystalline EMT particles after 36 hours of heating at 30°C (Fig. 3). We did not observe any difference between the TEM pictures of samples heated for 8 and 14 hours. Amorphous objects of about equal size with a diameter of 2 to 10 nm were seen in these samples (Fig. 3A); some of these particles had a size and morphology similar to the final EMT crystallites. The XRD pattern of the sample heated only for 8 hours did not exhibit any Bragg peaks, confirming the amorphous nature (Fig. 2A), whereas analysis of the diffraction pattern for the sample heated for 14 hours (Fig. 2B) resulted in nonsatisfactory fitting based on the use of one phase only (either amorphous or crystalline). Thus, we used a mixture of amorphous and nanocrystalline EMT-type zeolite for the fitting. On the basis of this refinement (Fig. 2B), the relative amount of the crystalline phase calculated is ~30%. More developed anisotropy of both unit-cell (c/a = 1.44) and mean crystallite shape (2.1 × 2.3 × 1.0 nm^3) was calculated for this sample based on the XRD. Although the XRD pattern corresponds to an entirely amorphous sample, based on the Rietveld refinement, we concluded that the particles had anisotropic shapes with mostly developed hexagonal platelike morphology (fig. S4 and table S2) (*28*). Moreover, the refined crystallite volume was comparable to the unit-cell volume, which is a signature of the starting of EMT growth (fig. S5). After 24 hours of heating, ultrasmall crystallites of zeolite EMT appeared in the amorphous matrix (Fig. 3B). The XRD pattern of this sample contains amorphous matter and low intense Bragg peaks (Fig. 2C). The size of the crystalline domains calculated based on XRD is 5.5 × 2.0 × 5.1 nm^3 (table S3). Moreover, the crystalline particles existing in the aluminosilicate system after 14 and 24 hours heating at 30°C already exhibited the hexagonal shape (insets in Fig. 2, B and C).

As the crystallization proceeded, the intensity of the Bragg peaks increased, but they were still broad because of the small crystalline domains. After 36 hours of heating, the amorphous particles were turned entirely into crystalline matter, as demonstrated with HRTEM and XRD (Figs. 2D and 3C). In the fully crystalline sample, we detected well-formed hexagonal particles with crystalline fringes. A closer look at these nanocrystals (Fig. 1) revealed that the apparent size and the hexagonal arrangement of the micropores correspond to the EMT-type zeolite. Further evidence for the high crystallinity of the samples was provided by N_2 sorption and spectroscopic data (infrared and nuclear magnetic resonance spectroscopy) (figs. S6 to S9 and table S4). The nitrogen sorption measurement of the fully crystalline sample (36 hours) revealed a type I sorption isotherm; micropores of 7.3 Å were observed in addition to textural mesoporosity (pores of 2 to 50 nm) attributed to the random packing of the ultrasmall nanocrystals. The Brunauer-Emmett-Teller surface area for the ultrasmall and nanosized EMT materials was 578 and 562 m^2/g, and the pore volume was 0.78 and 0.84 cm^3/g, respectively (table S4).

We compared the ultrasmall EMT crystals synthesized under conventional heating (Fig. 4, A and B) with nanosized EMT crystals synthesized under microwave heating (Fig. 4, C and D) at 30°C. The HRTEM images of the sample prepared with microwave treatment revealed the presence of small EMT crystals with the characteristic hexagonal platelike morphology (Fig. 4C). The crystalline solids showed a uniform particle size of 50 to 70 nm (Fig. 4D and figs. S1 and S10). The selected-area electron diffraction (SAED) pattern of the nanosized EMT exhibits sixfold symmetry, which is indicative of the EMT structural features (Fig. 4F and table S5). The distance between two fringes based on the TEM measurement is 1.3 nm. The ABABAB stacking of the faujasite sheets is observed in the EMT nanocrystals; this stacking gives the hexagonal crystal shape and EMT topology (Fig. 4E). Unlike high silica micrometer-sized EMT zeolite, the nanosized EMT grow favorably in the a direction, rather

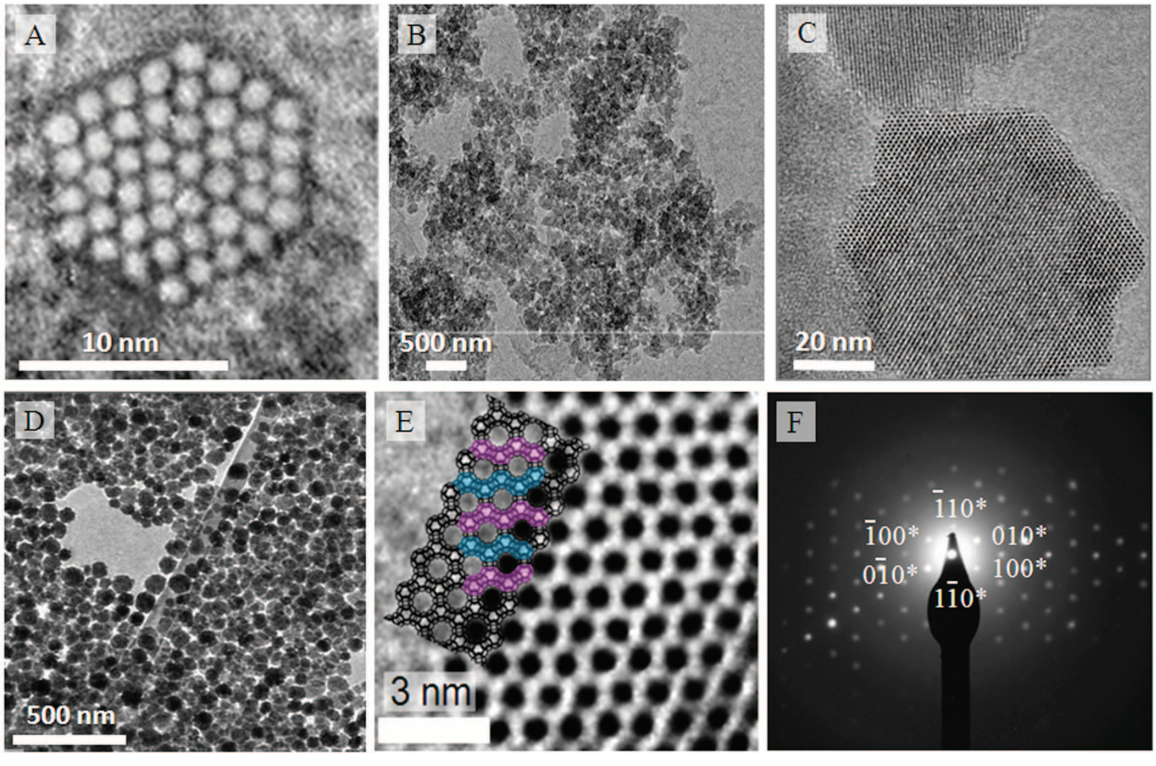

Fig. 4. TEM images of ultrasmall EMT crystals at different magnifications with scale bars of (**A**) 10 nm and (**B**) 500 nm, as well as nanosized EMT single crystals with scale bars of (**C**) 20 nm and (**D**) 500 nm. (**E**) Magnified TEM image and corresponding schematic diagram of the framework structure (ABABA stacking of faujasite sheets highlighted in purple and blue). (**F**) SAED pattern of a nanosized EMT single crystal, projected along [100].

than in the *c* direction, thus resulting in the thin hexagonal-plate form due to the limited crystal growth via the layer-by-layer mechanism along the *c* direction (*29*).

The homogeneity of the two samples, ultrasmall (6- to 15-nm) and nanosized (50- to -70 nm) EMT crystals, is illustrated at two different magnifications in Fig. 4, A to D. The hexagonal morphology of both samples is evident. Moreover, their colloidal stability was examined by measuring the zeta potential values, which are equal to –45 mV. This negative charge leads to electrostatic stabilization of the hexagonal nanoparticles.

Why has EMT never been observed in organic-free synthesis solutions? The reason may be surprisingly simple. When the same synthesis solutions as described above were heated at the same temperature for extended times or at higher temperatures, the nanoscale EMT materials converted into the well-known FAU and SOD structures (fig. S2). We propose that under appropriate conditions the EMT is the first kinetic, metastable product in this synthesis field, followed by conversion into the more stable cubic FAU and more dense SOD structures. This hypothesis is strongly supported by several reports on EMT/FAU intergrowths (*9*–*14*). Indeed, we suggest that it may be possible to capture other important zeolite phases that occur as intergrowths by exploiting the very early stages of synthesis and thus avoiding the use of organic reagents that are commonly needed to stabilize the desired phases.

From an environmental perspective, the synthesis of EMT zeolite presented here is extremely attractive, as the nanocrystals can be easily synthesized at very high yield at near ambient temperature without using any organic templates, suggesting that scale-up of an energy-efficient synthesis would be easily feasible. These nanoscale EMT materials offer exciting opportunities for both fundamental study and potential industrial applications. The possible green mass production of EMT-type zeolite provides excellent opportunities for applications in catalysis, adsorption, and separations involving larger molecules and for designing thin films, membranes, or nanoscale devices.

References and Notes

1. M. E. Davis, *Nature* **417**, 813 (2002).
2. D. W. Breck, *Zeolites and Molecular Sieves System* (Wiley, New York, 1974).
3. J. Choi *et al.*, *Science* **325**, 590 (2009).
4. M. A. Snyder, M. Tsapatsis, *Angew. Chem. Int. Ed.* **46**, 7560 (2007).
5. Ch. Baerlocher, L. B. McCusker, D. H. Olson, in *Atlas of Zeolite Framework Types* (Elsevier, Amsterdam, Netherlands, ed. 6, 2007), p. 123.
6. D. E. W. Vaughan, in *Properties and Applications of Zeolites*, R. P. Townsend, Ed. (The Chemical Society, London, 1980), p. 294.
7. F. Dougnier, J. Patarin, J.-L. Guth, D. Anglerot, *Zeolites* **12**, 160 (1992).
8. S. Liu, L. Li, C. Li, X. Xiong, F.-S. Xiao, *J. Porous Mater.* **15**, 295 (2008).
9. A. Haas, D. A. Harding, J. R. D. Nee, *Microporous Mesoporous Mater.* **28**, 325 (1999).
10. M. G. Barrett, D. E. W. Vaughan, UK Patent GB 2,076,793 A (1981).
11. D. E. W. Vaughan, European Patent 0,351,461 (1989).
12. J. M. Newsam, M. M. J. Treacy, D. E. W. Vaughan, K. G. Strohmaier, W. J. Mortier, *Chem. Commun.* 493 (1989).
13. G. T. Kokotailo, J. Ciric, *Adv. Chem. Ser.* **101**, 109 (1971).
14. J. A. Martens, P. A. Jacobs, S. Cartlidge, *Zeolites* **9**, 423 (1989).
15. F. Dougnier, J. L. Guth, *Microporous Mater.* **6**, 79 (1996).
16. R. Wendelbo, M. Stöcker, H. Junggreen, H. B. Mostad, Norwegian Patent Application No. 964988 (2001).
17. R. Wendelbo, M. Stöcker, H. Junggreen, H. B. Mostad, D. E. Akporiaye, *Microporous Mesoporous Mater.* **28**, 361 (1999).
18. M. Matsukata, K. Kizu, M. Ogura, E. Kikuchi, *Cryst. Growth Des.* **1**, 509 (2001).
19. J. Sun, M. Sun, C. Nie, Q. Li, *J. Chem. Soc. Chem. Commun.* 2459 (1999).
20. Y. Luo, J. Sun, W. Zhao, J. Yao, Q. Li, *Chem. Mater.* **14**, 1906 (2002).
21. T. Chatelain, J. Patarin, M. Soulard, J. L. Guth, P. Shulz, *Zeolites* **15**, 90 (1995).
22. S. L. Burkett, M. E. Davis, *Microporous Mater.* **1**, 265 (1993).
23. S. Mintova, N. H. Olson, V. Valtchev, T. Bein, *Science* **283**, 958 (1999).
24. B.-Z. Zhan *et al.*, *Chem. Mater.* **14**, 3636 (2002).
25. S. Mintova, M. Reinelt, T. H. Metzger, J. Senker, T. Bein, *Chem. Commun.* **2003**, 326 (2003).
26. L. Tosheva, V. Valtchev, *Chem. Mater.* **17**, 2494 (2005).
27. J. L. Casci, *Microporous Mesoporous Mater.* **82**, 217 (2005).
28. A. Le Bail, *J. Non-Cryst. Solids* **183**, 39 (1995).
29. G. González, C. S. González, W. Stracke, R. Reichelt, L. García, *Microporus Mesoporus Mater.* **101**, 30 (2007).
30. D. Chateigner, in *Combined Analysis: Structure-Texture-Microstructure-Phase-Stresses-Reflectivity Determination by X-ray and Neutron Scattering* (Wiley, New York, 2010), p. 410.
31. L. Lutterotti, S. Matthies, H.-R. Wenk, in *MAUD (Material Analysis Using Diffraction): A User Friendly JAVA Program for Rietveld Texture Analysis and More*, in *Textures of Materials*, J. A. Szpunar, Ed. (National Research Council Canada Research Press, Ottawa, 2002), p. 1599.
32. N. C. Popa, *J. Appl. Cryst.* **31**, 176 (1998).

Acknowledgments: We thank S. Schmidt (LMU) for collecting the TEM data and SRIF-ANR-06-NANO-007-01 Region and FEDER of Down Normandy, NIM (Nano-Initiative-Munich), for financial support.

Supporting Online Material

www.sciencemag.org/cgi/content/full/science.1214798/DC1
SOM Text
Figs. S1 to S12
Tables S1 to S5

3 October 2011; accepted 11 November 2011
Published online 8 December 2011;
10.1126/science.1214798

An Exhumation History of Continents over Billion-Year Time Scales

Terrence J. Blackburn,[1]* Samuel A. Bowring,[1] J. Taylor Perron,[1] Kevin H. Mahan,[2] Francis O. Dudas,[1] Katherine R. Barnhart[2]

The continental lithosphere contains the oldest and most stable structures on Earth, where fragments of ancient material have eluded destruction by tectonic and surface processes operating over billions of years. Although present-day erosion of these remnants is slow, a record of how they have uplifted, eroded, and cooled over Earth's history can provide insight into the physical properties of the continents and the forces operating to exhume them over geologic time. We constructed a continuous record of ancient lithosphere cooling with the use of uranium-lead (U-Pb) thermochronology on volcanically exhumed lower crustal fragments. Combining these measurements with thermal and Pb-diffusion models constrains the range of possible erosion histories. Measured U-Pb data are consistent with extremely low erosion rates persisting over time scales approaching the age of the continents themselves.

The preservation of fragments of stable Archean continental lithosphere, or "cratons," over geologic time is intimately linked with the presence of a low-density mantle root that supports and protects the overlying crust (*1*). The long-term stability of these roots has been attributed to an apparent "isopycnic" balance between the negative thermal buoyancy from contraction during cooling and the positive chemical buoyancy from the depletion of the root's denser basaltic component during craton formation (*1*, *2*). Despite this stability, cratons must survive exposure to surface processes working to erode on durations lasting billions of years, a process that results in continued rock exhumation toward Earth's surface. Although present-day erosion within these stable regions is low, the assembly of continental masses through mountain-building processes (*3*) requires that these terranes experienced periods of rapid erosion after the construction of topographically high mountain belts. An erosional history recording the duration of this early rapid erosional phase and the timing and rate of transition to the slow erosion observed today will allow us to understand more about the composition and density of the lithosphere, its relationship with the underlying mantle, and the thermal, buoyant, and mechanical forces operating to exhume or bury the continents over the geologic history of Earth.

Because the exhumation or burial of Earth's surface has a direct effect on the rate of heat loss within the lithosphere, a continuous record

[1]Earth Atmospheric and Planetary Sciences, Massachusetts Institute of Technology, Cambridge, MA 02139, USA. [2]Department of Geological Sciences, University of Colorado, Boulder, CO 80309, USA.

*To whom correspondence should be addressed. E-mail: terrence@mit.edu